

Science and Technology of Advanced Materials

ISSN: 1468-6996 (Print) 1878-5514 (Online) Journal homepage: www.tandfonline.com/journals/tsta20

Rapid growth of a pit-free (011) β-Ga_2O_3 homoepitaxial layer with very low residual Si and Cl concentrations by HCl-based halide vapor phase epitaxy

Yuichi Oshima & Takayoshi Oshima

To cite this article: Yuichi Oshima & Takayoshi Oshima (2026) Rapid growth of a pit-free (011) β-Ga_2O_3 homoepitaxial layer with very low residual Si and Cl concentrations by HCl-based halide vapor phase epitaxy, Science and Technology of Advanced Materials, 27:1, 2751773, DOI: 10.1080/14686996.2026.2751773

To link to this article: https://doi.org/10.1080/14686996.2026.2751773

© 2026 The Author(s). Published by National Institute for Materials Science in partnership with Taylor & Francis Group.

View supplementary material

Published online: 09 Nov 2026.

Submit your article to this journal

Article views: 256

View related articles

View Crossmark data

Full Terms & Conditions of access and use can be found at
https://www.tandfonline.com/action/journalInformation?journalCode=tsta20

SCIENCE AND TECHNOLOGY OF ADVANCED MATERIALS
2026, VOL. 27, NO. 1, 2751773
https://doi.org/10.1080/14686996.2026.2751773

Taylor & Francis
by informa

OPEN ACCESS Check for updates

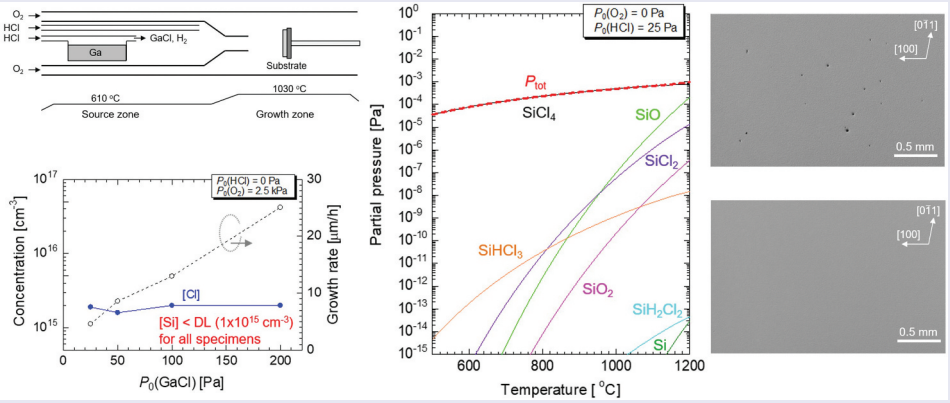
Rapid growth of a pit-free (011) β-Ga_2O_3 homoepitaxial layer with very low residual Si and Cl concentrations by HCl-based halide vapor phase epitaxy

Yuichi Oshima and Takayoshi Oshima

Research Center for Electronic and Optical Materials, National Institute for Materials Science, Tsukuba, Japan

ABSTRACT

We report the rapid growth of pit-free (011) β-Ga_2O_3 homoepitaxial layers with very low residual [Si] and [Cl] by HCl-based halide vapor phase epitaxy (HCl-HVPE) in which GaCl was generated from Ga and HCl. Along with the GaCl and O_2 growth precursors, additional HCl was introduced directly into the growth zone to suppress parasitic gas-phase reactions. The effects of O_2 and additional HCl partial pressures on residual impurity concentrations were systematically investigated. The [Si] decreased sharply with increasing O_2 partial pressure before reaching saturation, whereas it increased monotonically with additional HCl partial pressure and fell below the secondary ion mass spectrometry detection limit (1×10^{15} cm^{-3}) in the absence of additional HCl. Thermodynamic analysis of SiO_2 etching by H_2 and HCl qualitatively reproduced these trends and suggested that residual Si originates predominantly from HCl-induced etching of quartz components in the source zone in the reactor. Even without additional HCl, increasing the GaCl supply enabled a growth rate of 13 μm/h, comparable to that previously achieved with additional HCl, while maintaining [Si] below the detection limit and [Cl] below 2×10^{15} cm^{-3}, without particle-induced surface degradation. Furthermore, no pit formation was observed in the absence of additional HCl, and the pits were found to originate from substrate pre-etching by additional HCl before growth. These findings demonstrate that HCl-HVPE enables rapid homoepitaxy of pit-free (011) β-Ga_2O_3 layers with very low residual impurity concentrations, offering a promising route toward cost-effective vertical β-Ga_2O_3 power devices.



Impact Statement

This study identified the origins of residual Si contamination and pit formation in HCl-HVPE and demonstrates rapid growth of pit-free (011) β-Ga_2O_3 homoepitaxial layers with very low residual donor concentrations.

ARTICLE HISTORY
Received 28 July 2026
Revised 4 October 2026
Accepted 15 October 2026

KEYWORDS
β-Ga_2O_3; HVPE; impurity

Introduction

β-Ga_2O_3 is the most thermodynamically stable polymorph of Ga_2O_3 and possesses an ultra-wide bandgap of 4.5–4.9 eV [1,2]. Owing to its wide bandgap, β-Ga_2O_3 is expected to exhibit a high critical electric field [3]. Furthermore, large-area, high-quality single-crystal substrates grown by melt-growth techniques are commercially available, enabling homoepitaxial growth [4–10]. These advantages have established β-Ga_2O_3 as one of the most promising semiconductor materials for next-generation high-performance power electronics. Indeed, high-performance prototype devices, including Schottky barrier diodes

CONTACT Yuichi Oshima OSHIMA.Yuichi@nims.go.jp Research Center for Electronic and Optical Materials, National Institute for Materials Science (NIMS), 1-1 Namiki, Tsukuba, Ibaraki 305-0044, Japan

Supplemental data for this article can be accessed online at https://doi.org/10.1080/14686996.2026.2751773

© 2026 The Author(s). Published by National Institute for Materials Science in partnership with Taylor & Francis Group.
This is an Open Access article distributed under the terms of the Creative Commons Attribution License (http://creativecommons.org/licenses/by/4.0/), which permits unrestricted use, distribution, and reproduction in any medium, provided the original work is properly cited. The terms on which this article has been published allow the posting of the Accepted Manuscript in a repository by the author(s) or with their consent.

(SBDs) [11–14] and metal–oxide–semiconductor field-effect transistors (MOSFETs) [15–19], have already been demonstrated.

For high-voltage β-Ga_2O_3 power devices, the drift layer is required to be both thick and lightly doped. For example, realizing a device with a breakdown voltage of approximately 10 kV requires a drift layer with a thickness of 30–50 μm and a carrier concentration as low as 5×10^{15} – 1×10^{16} cm^{-3} [20]. Therefore, an epitaxial growth technique for high-voltage β-Ga_2O_3 power devices must provide both a high growth rate for cost-effective fabrication and a residual carrier concentration sufficiently lower than the required carrier concentration. Halide vapor phase epitaxy (HVPE) is a promising epitaxial growth technique potentially capable of meeting these requirements.

HVPE of β-Ga_2O_3 can be broadly classified into two types according to the method used to generate the GaCl precursor. One approach employs the reaction of metallic Ga with Cl_2 gas to produce GaCl and is hereafter referred to as Cl_2-HVPE. A notable advantage of Cl_2-HVPE is its extremely low residual [Si], which is typically below the secondary ion mass spectrometry (SIMS) detection limit (DL), for example, $<5 \times 10^{15}$ cm^{-3} [21]. Consequently, Cl_2-HVPE has been employed in most demonstrations of vertical β-Ga_2O_3 power devices [12–14,16,17,19]. However, increasing the precursor concentration to achieve higher growth rates tends to promote parasitic gas-phase reactions, resulting in particle formation [22]. As a result, commercially available (001) β-Ga_2O_3 epitaxial wafers are typically grown at a relatively low growth rate of approximately 4 μm/h [20].

The other type of HVPE employs the reaction of metallic Ga with HCl gas to generate the GaCl precursor and is hereafter referred to as HCl-HVPE to distinguish it from Cl_2-HVPE according to the chlorine source. A characteristic feature of HCl-HVPE is the simultaneous generation of H_2 as a by-product during GaCl formation. In GaN grown by HCl-HVPE, relatively high residual [Si] (typically on the order of 10^{17} cm^{-3} [23]) have been widely reported. This has been attributed to etching of the quartz reactor components, which are extensively used in HVPE reactors, by H-containing gases (H_2, HCl, and NH_3), resulting in the generation of Si-containing gaseous species. Indeed, it has been reported that the residual [Si] can be reduced to below 5×10^{14} cm^{-3} by eliminating quartz components from the HVPE reactor [23]. By analogy with these findings for GaN, HCl-HVPE has generally been considered more susceptible than Cl_2-HVPE to Si contamination in β-Ga_2O_3 epilayers [24]. On the other hand, HCl-HVPE generally enables higher growth rates than Cl_2-HVPE [25–27]. This is presumably because the H_2 generated during growth, which also acts as an etchant for β-Ga_2O_3, suppresses particle formation caused by parasitic reactions between the source gases. Furthermore, the growth rate in HCl-HVPE can be further increased by introducing additional HCl into the growth zone [26,28,29]. For example, we routinely achieve a high growth rate of 24 μm/h for (001) β-Ga_2O_3 growth using HCl-HVPE with additional HCl [26,28].

To date, (001)-oriented substrates have been predominantly used for the epitaxial growth of β-Ga_2O_3 drift layers for vertical power devices. This is mainly because the (001) plane is parallel to the [010] pulling direction used in the edge-defined film-fed growth (EFG) method, facilitating the fabrication of large-area substrates, and because it generally allows higher HVPE growth rates than other crystal orientations [30]. However, a common drawback of (001) homoepitaxy by both types of HVPE is the relatively high residual [Cl], with typical values around 1×10^{16} cm^{-3} [20,26,31]. One promising approach to overcoming this issue is to employ the (011) orientation. For both Cl_2-HVPE and HCl-HVPE, the residual [Cl] in (011) epilayers has been reported to be approximately one order of magnitude lower than that in (001) epilayers [26,32]. However, the growth rate on the (011) plane is only about 60% of that on the (001) plane and is as low as approximately 2 μm/h for Cl_2-HVPE [32]. Nevertheless, several promising vertical β-Ga_2O_3 power devices based on (011) epilayers have been demonstrated [19,33,34]. For example, Wakimoto et al. reported a FinFET with a breakdown voltage exceeding 10 kV incorporating an 85-μm-thick drift layer grown by Cl_2-HVPE [19].

In contrast, HCl-HVPE with additional HCl has been reported to achieve a much higher growth rate of 14 μm/h than that reported for Cl_2-HVPE, while maintaining a low residual [Cl] of 1.7×10^{15} cm^{-3}. However, the residual [Si] remains relatively high at 2×10^{16} cm^{-3} [26]. Another issue is the formation of pits on the epilayer surface at a density of approximately 10^3–10^4 cm^{-2}, a phenomenon that has not been reported for Cl_2-HVPE [26]. These pits extend nearly to the epilayer/substrate interface, suggesting that their origin is associated with the epilayer/substrate interface.

If the residual [Si] and pit formation on the (011) surface can be effectively suppressed, HCl-HVPE could become a promising epitaxial growth technique for β-Ga_2O_3 power devices by combining high growth rates with the intrinsic advantage of low Cl incorporation. In this work, we investigate the origins of residual Si incorporation and pit formation in HCl-HVPE. Furthermore, we demonstrate rapid homoepitaxial growth of pit-free (011) β-Ga_2O_3 with a residual [Si] below the SIMS detection limit while maintaining the low residual [Cl] characteristic of the (011) orientation.

Experimental methods

(011) β-Ga_2O_3 homoepitaxial growth was carried out by atmospheric-pressure HVPE at 1030°C without intentional doping on conductive Sn-doped (011) β-Ga_2O_3 single-crystal substrates grown by the EFG method (Novel Crystal Technology, Inc.) using a laboratory-built quartz reactor. A schematic illustration of the HVPE reactor is shown in Figure 1. Not only the main reactor tube but also all internal components were made of quartz. High-purity O_2 gas (>99.99995%) was used as the oxygen source. GaCl precursor gas was generated in the source zone maintained at 610°C by reacting metallic Ga (>99.99999%) with source HCl gas (>99.999%) in the Ga boat. Under these conditions, the source HCl was essentially completely consumed and converted into GaCl and H_2. In addition to the precursor gases, the reactor was equipped with a supply line for additional HCl gas to suppress parasitic reactions between the source gases [26,29]. Unlike the source HCl, the additional HCl bypassed the Ga boat without reacting with metallic Ga and was introduced directly into the growth zone. N_2 gas (dew point < −110 °C) was used as the carrier gas for all gas streams. The GaCl and additional HCl gas streams were transported independently of the O_2 gas stream and mixed only in the growth zone, where β-Ga_2O_3 growth took place. No intentional post-growth annealing was performed.

During the temperature ramp-up, O_2 was supplied at the same partial pressure as that used during the growth step. After the reactor temperature had stabilized, the GaCl supply was initiated to start epitaxial growth. When additional HCl was used, its supply was started 5 min before the introduction of GaCl. Consequently, the β-Ga_2O_3 substrates were subjected to a slight etching treatment prior to growth.

The growth rate was determined from the substrate weight change before and after epitaxial growth. The surface morphology was characterized by Nomarski optical microscopy using BX51 (OLYMPUS, Japan) and scanning electron microscopy (SEM) using SU8230 (Hitachi, Japan). Impurity concentrations were measured by SIMS.

To confirm that the residual carrier concentration was sufficiently reduced, a SBD consisting of an unintentionally doped homoepitaxial layer grown on a conductive Sn-doped (011) β-Ga_2O_3 substrate was fabricated. Its current–voltage (J–V) and capacitance–voltage (C–V) characteristics were measured using a semiconductor parameter analyzer B1500A (Keysight, US). The C–V measurement was performed at an AC frequency of 1 MHz, assuming a relative dielectric constant of 10 for β-Ga_2O_3. For the cathode, Ti (30 nm)/Pt (20 nm)/Au (70 nm) contacts were deposited by electron-beam (EB) evaporation, followed by rapid thermal annealing (RTA) at 550°C for 1 min in N_2 gas flow. The ohmic behavior of the backside contact was confirmed by the linear I–V characteristics measured between adjacent cathode electrodes. The Schottky anode consisted of a 50-nm-thick Au electrode with an area of 2.3×10^{-3} cm^2 was deposited by EB evaporation.

Results and discussion

Figure 2(a) shows the dependences of the residual [Si] and [Cl], and growth rate on the supplied O_2 partial pressure, $P_0(O_2)$. Here, $P_0(X)$ denotes the supplied partial pressure of gas species X. Note that P_0(HCl) hereafter refers to the partial pressure of the additional HCl rather than that of the source HCl. Throughout this experiment, both P_0(GaCl) and P_0(HCl) were fixed at 25 Pa. The growth rate increased with increasing $P_0(O_2)$, gradually approaching saturation. The residual [Si] was 1.5×10^{16} cm^{-3} at the lowest $P_0(O_2)$ investigated but decreased rapidly to 3.2×10^{15} cm^{-3}, approximately one-fifth of the initial value, at $P_0(O_2)$ = 0.625 kPa. A further increase in $P_0(O_2)$ produced little change in the residual [Si]. In contrast, the residual [Cl] exhibited a slight increase with increasing $P_0(O_2)$, while remaining as low as 1.5×10^{15} cm^{-3} even at the highest $P_0(O_2)$ investigated. Considering that Cl is generally believed to occupy O sites in β-Ga_2O_3 [35], one might expect the Cl incorporation to decrease with increasing P_0 (O_2). However, the opposite trend was observed. This result suggests that Cl incorporation is influenced by mechanisms other than simple competition between O and Cl for O lattice sites. The origin of this behavior remains unclear at present and requires further investigation.

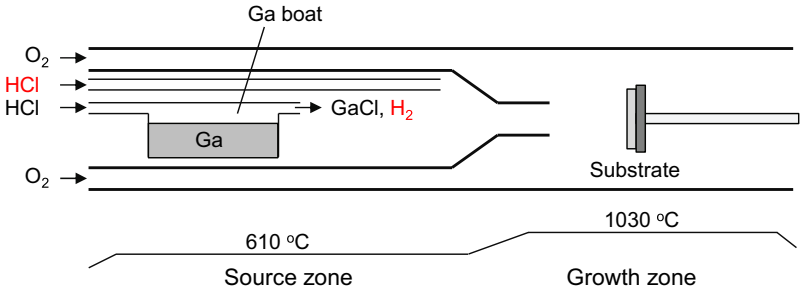


Figure 1. Schematic of the HVPE reactor used in this study. Carrier gas flows are omitted for clarity.

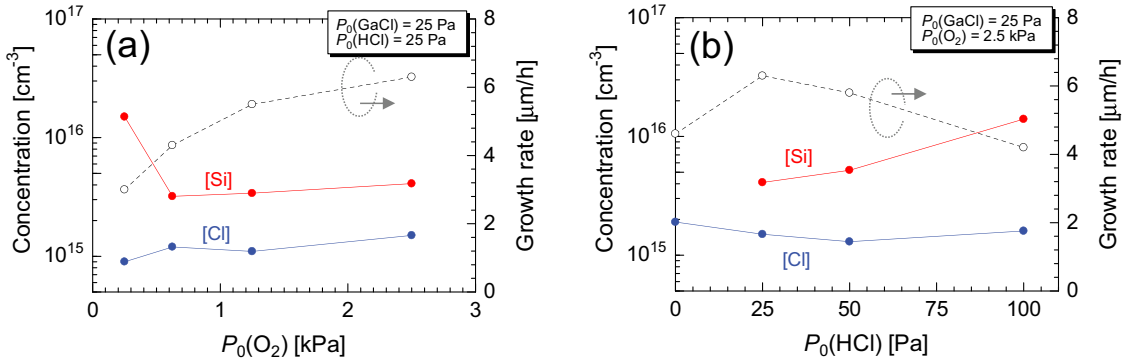


Figure 2. Dependences of the residual [Si] and [Cl], and growth rate on (a) $P_0(O_2)$ and (b) P_0(HCl).

Figure 2(b) shows the dependences of the residual [Si] and [Cl], and the growth rate on P_0(HCl). In this experiment, P_0(GaCl) and $P_0(O_2)$ were fixed at 25 Pa and 2.5 kPa, respectively. The growth rate initially increased with increasing P_0(HCl) and then gradually decreased. This behavior is considered to result from two competing effects. At low P_0(HCl), the additional HCl suppresses parasitic gas-phase reactions, thereby improving the transport efficiency of the source species to the substrate. At higher P_0(HCl), however, the etching of β-Ga_2O_3 on the substrate becomes dominant, resulting in a reduction in the net growth rate. When no additional HCl was supplied, the residual [Si] was below the SIMS detection limit (1×10^{15} cm^{-3}); therefore, this data point is not included in Figure 2(b). The residual [Si] increased monotonically with increasing P_0(HCl) and reached 1.4×10^{16} cm^{-3} at P_0(HCl) = 100 Pa. In contrast, the residual [Cl] exhibited no clear dependence on P_0(HCl) and remained nearly constant in the range of $(1.3–1.9) \times 10^{15}$ cm^{-3}.

As shown in Figure 2(a), the residual [Si] can be substantially reduced by increasing $P_0(O_2)$. This reduction is most likely attributable to the suppression of SiO_2 reduction by the H-containing species, H_2 and HCl, in the presence of O_2. A notable feature is that the residual [Si] did not decrease continuously with increasing $P_0(O_2)$. Instead, it dropped sharply with a relatively small increase in $P_0(O_2)$ and then remained nearly constant. This behavior suggests that even a relatively low O_2 partial pressure is sufficient to effectively suppress the reduction of SiO_2.

The monotonic increase in the residual [Si] with increasing P_0(HCl), shown in Figure 2(b), further suggests that HCl plays a significant role in etching SiO_2 and thereby enhances Si contamination. It should be noted that, even in the absence of additional HCl, H_2 generated during GaCl formation was still present in the reactor at a partial pressure of one-half that of P_0(GaCl) (12.5 Pa). If H_2 had an etching effect on SiO_2 comparable to or greater than that of HCl under the present growth conditions, a detectable concentration of Si would also be expected even without additional HCl. However, the residual [Si] remained below the SIMS detection limit. These results therefore suggest that, under the present growth conditions, the effective etching capability of H_2 toward SiO_2 was weaker than that of HCl.

To elucidate the experimentally observed behavior of the residual [Si], the thermodynamic driving forces for SiO_2 etching by H_2 and HCl were evaluated, and their dependences on temperature and $P_0(O_2)$ were analyzed. The thermodynamic model and calculation procedure are described below. Assuming that the SiO_2 etching rate is governed primarily by the equilibrium generation of volatile Si-containing species, the thermodynamic driving force for SiO_2 etching is expected to correlate with the total equilibrium partial pressure of these species at the SiO_2 surface. Accordingly, the following quantity was adopted as an indicator of the etching driving force:

$$P_{tot} = \sum_i n_i P(Si_{n_i}X_i) \quad (1)$$

where $P(Si_{n_i}X_i)$ is the equilibrium partial pressure of a gaseous species $Si_{n_i}X_i$.

The equilibrium partial pressures of all gaseous species were calculated using the thermodynamic equilibrium software CatCalc (Research Institute of Computational Thermodynamics, Inc.), which determines the equilibrium gas composition by minimizing the Gibbs free energy of the system [36].

For the analysis of SiO_2 etching by H_2, the following gaseous species were included in the equilibrium calculation: Si, Si_2, Si_3, SiH_4, SiO, SiO_2, $Si(OH)_4$, SiH_2O_3, H_2, H_2O, H_2O_2, O_2, and O_3, together with inert carrier gas. For the analysis of SiO_2 etching by HCl, the following gaseous species were considered: Si, Si_2, Si_3, SiH_4, SiO, SiO_2, $Si(OH)_4$, SiH_2O_3, $SiCl_2$, $SiCl_4$, SiH_2Cl_2, SiH_3Cl, $SiHCl_3$, H_2, H_2O, H_2O_2, O_2, O_3, Cl_2, Cl_4, Cl_2O, ClO_2, HCl, HClO, and $HClO_4$, together with inert carrier gas.

For the H_2 etching calculations, $P_0(H_2)$ was fixed at 12.5 Pa, corresponding to the H_2 generated as a by-product during GaCl formation from metallic Ga and

source HCl under the growth conditions used for the experiments shown in Figure 2(a,b), where P_0(GaCl) was 25 Pa. For the HCl etching calculations, P_0(HCl) was fixed at 25 Pa, corresponding to the experimental conditions used in Figure 2(a). $P_0(O_2)$, was varied from 0 to 2.5 kPa to cover the experimental growth conditions.

Figure 3(a,b) show the calculated temperature dependences of the equilibrium partial pressures of individual volatile Si-containing species, $Si_{n_i}X_i$, and the etching driving force indicator, P_{tot}, for SiO_2 etching by H_2 ($P_0(H_2) = 12.5$ Pa) and HCl (P_0(HCl) = 25 Pa), respectively, under $P_0(O_2) = 0$. The vertical dashed lines indicate the source-zone temperature (610 °C) and the growth-zone temperature (1030 °C). The equilibrium partial pressures of the Si-containing species not shown are below the plotting range. The dominant volatile Si-containing species generated by H_2 and HCl etching are SiO and $SiCl_4$, respectively, and their equilibrium partial pressures almost completely overlap with the corresponding P_{tot} curves. A notable feature is that the temperature dependence of the etching driving force is much weaker for HCl than for H_2. Consequently, although the HCl-induced etching driving force is comparable to that for H_2 at the growth-zone temperature of 1030°C, it is much greater at the source-zone temperature of 610°C.

Figure 4(a,b) show the calculated temperature dependences of the etching driving force indicator, P_{tot}, for SiO_2 etching by H_2 ($P_0(H_2) = 12.5$ Pa) and HCl (P_0(HCl) = 25 Pa), respectively, in the presence of O_2.

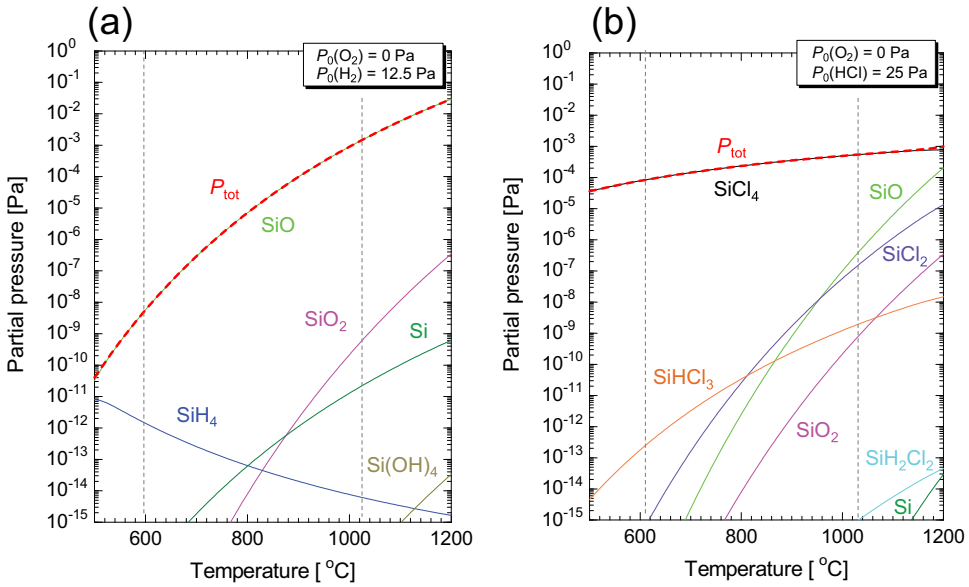


Figure 3. Calculated temperature dependences of the equilibrium partial pressures of Si-containing gaseous species and the etching driving force indicator, P_{tot}, for SiO_2 etching by (a) H_2 and (b) HCl.

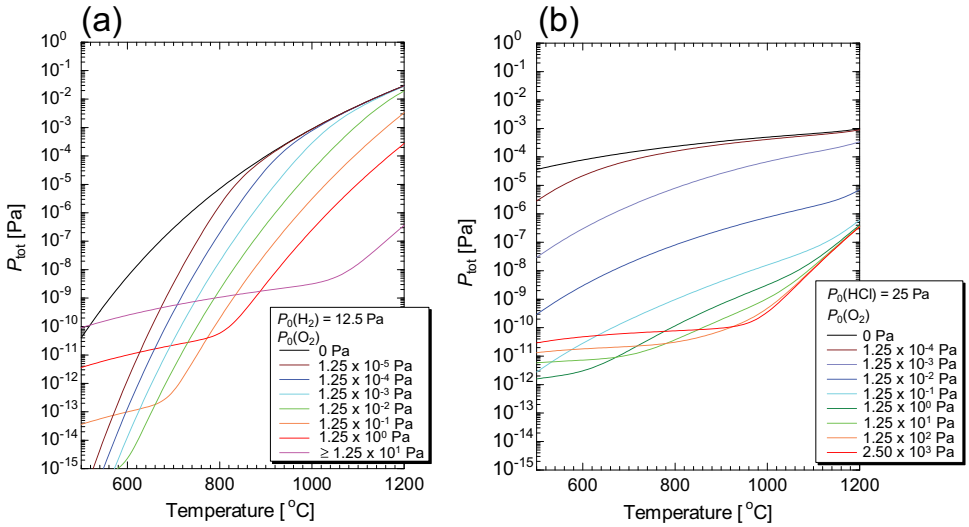


Figure 4. Calculated temperature dependences of the etching driving force indicator, P_{tot}, at various $P_0(O_2)$: (a) H_2 etching and (b) HCl etching.

For both etchants, P_{tot} decreases markedly with O_2 supply. In Figure 4(a), the P_{tot} curves for $P_0(O_2)$ ≥12.5 Pa almost completely overlap. It should also be noted that the dominant volatile Si-containing species depend on $P_0(O_2)$. Under the standard experimental condition of P_0 (O_2) = 2.5 kPa, $Si(OH)_4$ becomes the dominant Si-containing species for both H_2 and HCl etching, in contrast to the O_2-free case. The calculated temperature dependences of the equilibrium partial pressures of individual Si-containing species and P_{tot} for various $P_0(O_2)$ values are presented in Figs. S1 and S2.

Figure 5(a,b) show the calculated dependences of P_{tot} on $P_0(O_2)$ at 1030°C for SiO_2 etching by H_2 (P_0 (H_2) = 12.5 Pa) and HCl (P_0(HCl) = 25 Pa), respectively. In both cases, P_{tot} decreases sharply even with a small O_2 supply. For example, in the H_2 etching calculation, supplying O_2 at only one-tenth of the H_2 partial pressure ($P_0(O_2)$ = 1.25 Pa) reduces P_{tot} to less than one-thousandth of its value without O_2. These calculated results provide a qualitative explanation for the experimentally observed sharp decrease in the residual [Si] with a relatively small increase in $P_0(O_2)$, followed by the appearance of a plateau, as shown in Figure 2(a).

Table 1 compares the calculated etching driving forces for SiO_2 by H_2 and additional HCl in the source zone and the growth zone of the HVPE reactor. In the source zone, the etching driving force for additional HCl is much greater than that for H_2. This is because the etching driving force of HCl exhibits a much weaker temperature dependence than that of H_2, allowing HCl to maintain a high etching capability even at the relatively low source-zone temperature of 610°C.

In contrast, the etching driving forces in the growth zone are much smaller than that for additional HCl in the source zone for both etchants because of the strong suppression by O_2. These results therefore suggest that SiO_2 etching in the HVPE reactor is dominated by additional HCl in the source zone. This mechanism provides a qualitative explanation for the strong dependence of the residual [Si] on P_0(HCl) observed in Figure 2(b).

The experimental results described above demonstrated that the residual [Si] in (011) β-Ga_2O_3 homoepitaxial layers can be reduced below the SIMS detection limit by eliminating the supply of additional HCl. However, under these conditions, the growth rate was limited to 4.6 μm/h for P_0 (GaCl) = 50 Pa, which is considerably lower than the reported value of 14 μm/h for HVPE with additional HCl [26]. Therefore, the growth rate was increased by increasing P_0(GaCl) while maintaining $P_0(O_2)$ at 2.5 kPa. Figure 6(a) shows the dependences of the growth rate, the residual [Si] and [Cl] on P_0(GaCl). The labels (b) and (c) correspond to the SEM images shown in Figure 6(b,c), respectively. At P_0(GaCl) = 100 Pa [label (b)], the growth rate reached 13 μm/h, comparable to that reported for HVPE with additional HCl, while no degradation of the surface morphology was observed, as shown in Figure 6(b). When P_0(GaCl) was further increased to 200 Pa [label (c)], the growth rate increased to 25 μm/h. However, numerous particles were observed on the epilayer surface, as shown in

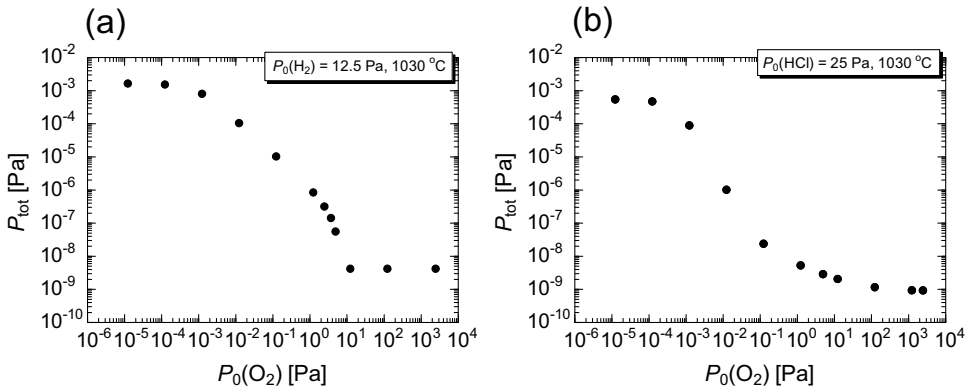


Figure 5. Calculated dependences of the etching driving force indicator, P_{tot}, on $P_0(O_2)$ at 1030°C for (a) H_2 etching and (b) HCl etching.

Table 1. Comparison of the etching driving force indicator, P_{tot}, for H_2 and HCl in the source and growth zones of the HVPE reactor.

Etchant	Source zone (610 °C) $P_0(O_2)$ = 0 kPa	Growth zone (1030 °C) $P_0(O_2)$ = 25 kPa
H_2 $P_0(H_2)$ = 12.5 Pa	8.8×10^{-14} Pa	4.1×10^{-14} Pa
HCl P_0(HCl) = 25 Pa	8.4×10^{-10} Pa	9.1×10^{-15} Pa

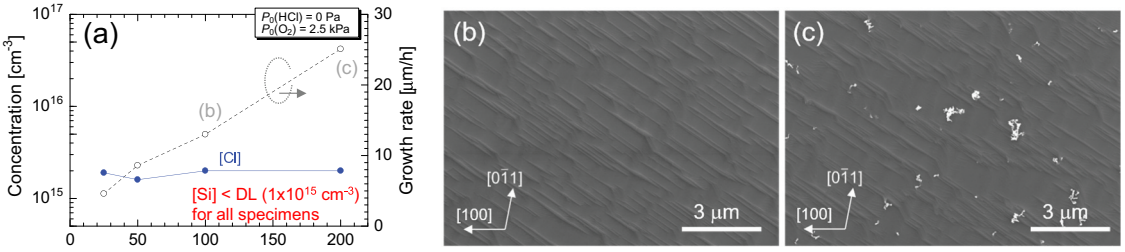


Figure 6. (a) Dependences of the residual [Cl] and growth rate on P_0(GaCl). The residual [Si] was below the SIMS detection limit under all growth conditions. (b), (c) corresponding plan-view SEM images of the epilayer surfaces grown at P_0(GaCl) = 100 and 200 Pa, respectively.

Figure 6. These particles were most likely generated by parasitic reactions between GaCl and O_2 under the high precursor concentration. To further increase the growth rate while suppressing particle formation, two approaches appear promising: supplying a small amount of additional HCl while maintaining the residual [Si] below the acceptable level, or employing reduced-pressure growth.

As also shown in Figure 6(a), no significant increase in the residual [Cl] was observed even at the highest growth rates, and the residual [Si] remained below the SIMS detection limit (1×10^{15} cm^{-3}) for all samples. In contrast, for the (001) orientation, a significant increase in the residual [Cl] has been reported for P_0 (GaCl) increase [26]. This difference suggests that, in addition to thermodynamic factors, crystal-orientation-dependent kinetic effects also play an important role in Cl incorporation. However, further studies are required to clarify the underlying mechanism.

The possible relationship between the surface morphology and residual impurity concentrations was also examined by comparing epilayers grown under different conditions. Although the surface morphology varied with the growth conditions, no systematic relationship was found between the surface morphology and the residual [Si] or [Cl]. This suggests that the residual impurity concentrations are not primarily correlated with the morphology of the flat regions.

To verify that the substantial reduction in both the residual [Si] and [Cl] achieved by eliminating additional HCl also resulted in a low carrier concentration, C–V and J–V measurements were performed on a SBD. A schematic cross-sectional structure of the SBD is shown in Figure 7(a), and an optical microscope image of the Schottky anode is shown in Figure 7(b). The homoepitaxial layer was grown under the same conditions as those of the sample shown in Figure 6(b), yielding [Si] $<1 \times 10^{15}$ cm^{-3} and [Cl] = 2×10^{15} cm^{-3}.

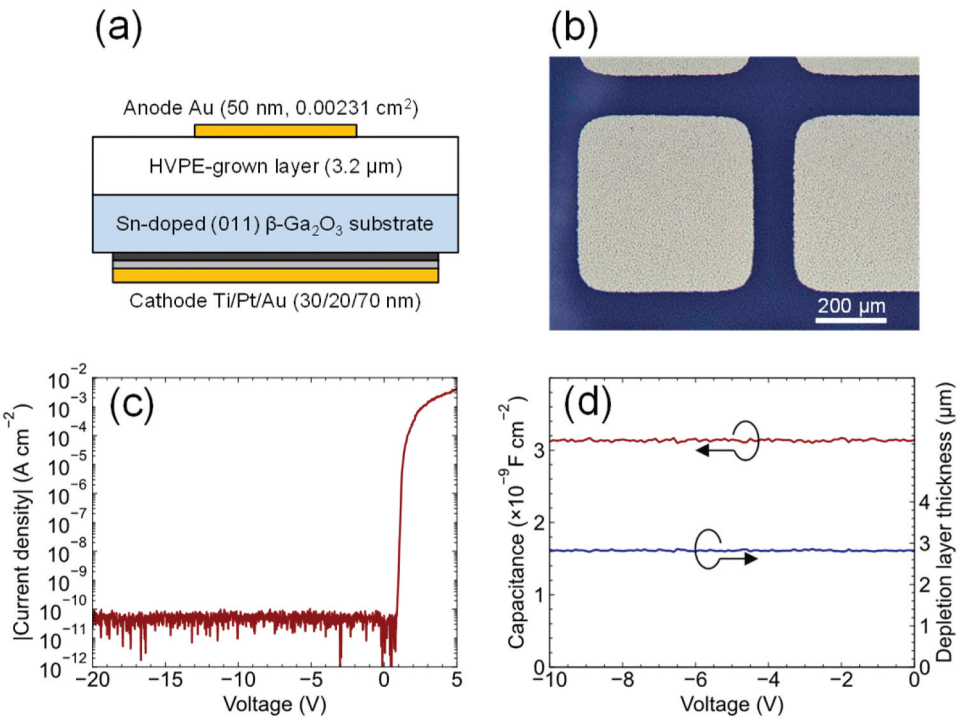


Figure 7. (a) Cross-sectional structure of the SBD used for the J–V and C–V measurements. (b) Optical microscope image of the Schottky anode. (c), (d) measured J–V and C–V characteristics, respectively.

Figure 7 shows the J–V characteristics of the SBD. The reverse leakage current was low, indicating good barrier characteristics. From the slope of the forward J–V curve above the turn-on voltage, the series resistance was estimated to be approximately 360 kΩ, indicating that the homoepitaxial layer was highly resistive. Because of this high series resistance, a substantial fraction of the applied voltage is expected to drop across the epilayer. Therefore, the forward J–V characteristics are not suitable for conventional extraction of the ideality factor and Schottky barrier height.

Figure 7 shows the C–V characteristics of the SBD at 1 MHz. The capacitance showed little dependence on the applied voltage. The depletion width estimated directly from the measured capacitance was approximately 3 μm, which is nearly equal to the epilayer thickness, indicating that the epilayer was nearly fully depleted. To examine whether the capacitance measurement was affected by the high series resistance or by insufficient response of slowly responding electrically active states at 1 MHz, C–V measurements were also performed at a lower frequency of 100 kHz. Similar voltage-independent capacitance and a depletion width close to the epilayer thickness were obtained at 100 kHz, consistent with the results obtained at 1 MHz. Assuming a built-in potential of 1 V, the $N_D - N_A$ required for complete depletion of the epilayer at this voltage was estimated to be at most 1.2×10^{14} cm^{-3}.

The estimated $N_D - N_A$ was considerably lower than the residual [Cl] of approximately 2×10^{15} cm^{-3}. The activation state of the residual Cl cannot be determined from the present results, and this discrepancy may arise from incomplete donor activation, compensation by unintentional acceptors, or both.

During the investigation of the dependence of the residual impurity concentrations on P_0(HCl), we found that additional HCl plays a critical role in pit formation on the epilayer surface. Figure 8(a) shows a Nomarski optical micrograph of a homoepitaxial layer grown for 1 h at a growth rate of 4.3 μm/h with $P_0(\mathrm{GaCl}) = P_0(\mathrm{HCl}) = 25$ Pa and $P_0(\mathrm{O_2}) = 2.5$ kPa. Numerous pits are observed, with a density of approximately 3.5×10^2 cm^{-2}. In contrast, no pits were observed in the homoepitaxial layer shown in Figure 8(b), which was grown for 1 h under the same precursor partial pressures without additional HCl at a comparable growth rate of 4.6 μm/h. Figure 8(c) shows a sample initially grown under the pit-free conditions used for Figure 8(b). After the epilayer thickness reached 2.3 μm, additional HCl was introduced so that the growth conditions became identical to those used for the sample shown in Figure 8(a), and growth was continued until the total thickness reached 4.5 μm. Nevertheless, almost no pits were observed. It should be noted that the residual [Si] in the upper part of the epilayer in Figure 8(c) should be the same as that in the epilayer shown in Figure 8(a), because they were grown under the same additional-HCl condition. Nevertheless, almost no new pits were formed in the epilayer shown in Figure 8(c). This result suggests that the increased Si incorporation itself is not the direct cause of pit formation. These results strongly suggest that pit formation is not caused by the presence of additional HCl during epitaxial growth itself, but rather by the pre-growth etching of the substrate surface by additional HCl before the introduction of GaCl.

Figure 9(a) shows a Nomarski optical micrograph of a (011) β-Ga_2O_3 substrate subjected only to HCl pre-etching under the same conditions as those used prior to the growth of the pit-containing sample shown in Figure 8(a). To more clearly reveal the surface morphology produced by etching, the etching time was increased to 50 min, which is ten times longer than that used in the growth experiments. Numerous hillocks with a density of approximately 1.1×10^4 cm^{-2} were observed, as indicated by the arrows.

Figure 9(b) shows a plan-view SEM image of one of these hillocks. An inclined facet plane, indicated by the arrow, is clearly visible. The trace direction of the facet on the (011) surface coincides with the intersection direction between the (011) and $(\bar{3}10)$ planes, i.e. the $[\bar{1}\bar{3}3]$ direction. Furthermore, the inclination angle of the facet, determined geometrically from the apparent change in facet width in tilted-view SEM observations, was 50.9°, which agrees almost exactly with the theoretical angle of 51.0° between the (011) and $(\bar{3}10)$ planes. These observations indicate that the facet is the $(\bar{3}10)$ plane. The $(\bar{3}10)$ plane is known to

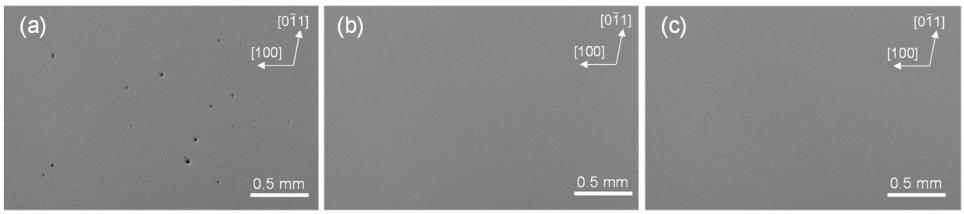


Figure 8. Nomarski optical micrographs of the surfaces of (011) β-Ga_2O_3 homoepitaxial layers grown (a) with additional HCl, (b) without additional HCl, and (c) with additional HCl introduced after an initial growth period without additional HCl.

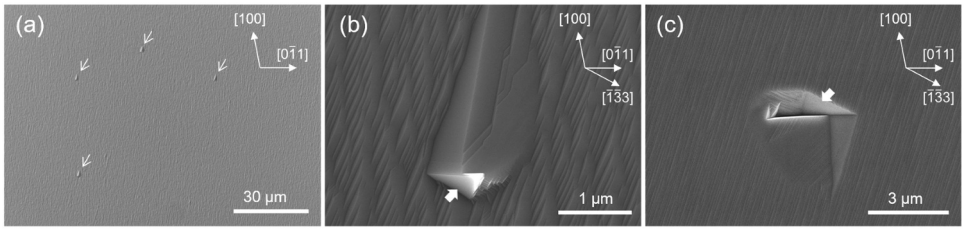


Figure 9. (a) Nomarski optical micrograph and (b) plan-view SEM image of an HCl-etched (011) β-Ga_2O_3 substrate. (c) Plan-view SEM image of a pit formed on a (011) β-Ga_2O_3 homoepitaxial layer during growth with additional HCl.

be one of the relatively stable low-surface-energy planes of β-Ga_2O_3 [37], and the formation of similar ($\bar{3}$10) facets has also been reported during selective HCl etching of (010) and (001) β-Ga_2O_3 substrates [38,39].

Figure 9 shows a plan-view SEM image of a pit formed on the homoepitaxial layer grown under additional-HCl supply. Nearly all of the observed pits were accompanied by the ($\bar{3}$10) facet, as indicated by the arrow. These results strongly suggest that HCl pre-etching of the (011) substrate produces stable ($\bar{3}$10) facets, which subsequently act as the origin of pit formation. Owing to their high stability, the growth rate on the ($\bar{3}$10) facets is presumably lower than that on the surrounding (011) surface. Consequently, the growth front above the facets lags behind the surrounding epilayer during homoepitaxy, while the ($\bar{3}$10) facets continue to develop, eventually leading to pit formation.

The dislocation density in EFG-grown β-Ga_2O_3 has been reported to be on the order of 10^3 cm^{-2} [20], which is reasonably close to the hillock density observed after HCl pre-etching. This may indicate that dislocations are involved in hillock formation. On the other hand, the pit density on the homoepitaxial surface was only approximately 3.5×10^2 cm^{-2}, much lower than the hillock density. This suggests that only a fraction of the hillocks develop into pits, possibly because only those with particularly well-developed ($\bar{3}$10) facets continue to evolve during subsequent epitaxial growth.

Conclusions

In summary, we experimentally clarified the effects of $P_0(O_2)$ and P_0(HCl) on the residual [Si] and [Cl] in (011) β-Ga_2O_3 homoepitaxial layers grown by HCl-HVPE. the residual [Si] exhibited a characteristic dependence on $P_0(O_2)$, decreasing sharply with a relatively small increase in $P_0(O_2)$ and subsequently remaining nearly constant. In addition, the residual [Si] was reduced below the SIMS detection limit (1×10^{15} cm^{-3}) in the absence of additional HCl, despite the presence of H_2 generated during GaCl formation, whereas it increased markedly with increasing P_0(HCl). In contrast, the residual [Cl] showed little dependence on either $P_0(O_2)$ or P_0(HCl) and remained below 2×10^{15} cm^{-3} throughout this study.

To explain these experimental observations, the thermodynamic driving force for SiO_2 etching was analyzed using the equilibrium parameter P_{tot}. The calculations revealed that the etching driving force of HCl is much less temperature dependent than that of H_2 under O_2-free conditions, allowing HCl to maintain a high etching capability even in the relatively low-temperature source zone (610°C). In contrast, the addition of a small amount of O_2 dramatically suppressed the etching driving force for both etchants, predicting that SiO_2 etching in the growth zone is much weaker than that by additional HCl in the source zone. These predictions consistently explain the experimentally observed strong correlation between the residual [Si] and P_0(HCl), the absence of detectable Si without additional HCl despite the presence of H_2, and the characteristic dependence of the residual [Si] on $P_0(O_2)$.

Furthermore, by eliminating additional HCl and increasing P_0(GaCl), a growth rate of 13 μm/h, comparable to that previously reported for HVPE with additional HCl, was achieved without particle formation or increases in the residual [Si] and [Cl]. *C–V* measurements of a SBD fabricated on such a homoepitaxial layer confirmed its semi-insulating nature, confirming that the residual carrier concentration was successfully reduced, although carrier compensation by unintentionally incorporated acceptors, such as nitrogen, is suggested. We also found that pit formation was dramatically suppressed in the absence of additional HCl and showed that the pits most likely originate from substrate pre-etching by additional HCl, which produces stable ($\bar{3}$10) facets before epitaxial growth.

Although HCl-HVPE of (011) β-Ga_2O_3 has been recognized as a promising technique capable of much higher growth rates than Cl_2-HVPE, its practical application has been hindered by high residual [Si] and pit formation. The present study demonstrates that both of these issues can be effectively overcome. These findings establish HCl-HVPE as a practical route for the high-rate growth of high-quality (011) β-Ga_2O_3 homoepitaxial layers and are expected to contribute significantly to the cost-effective manufacturing and widespread deployment of high-performance β-Ga_2O_3 power devices.

Acknowledgments

This work was supported by the 'Advanced Research Infrastructure for Materials and Nanotechnology in Japan (ARIM)' initiative of the Ministry of Education, Culture, Sports, Science and Technology (MEXT) under Proposal Numbers JPMXP1225NM5075 and JPMXP1226NM5276.

Disclosure statement

No potential conflict of interest was reported by the author(s).

Funding

This study was based on the results obtained from a project, JPNP22007, commissioned by the New Energy and Industrial Technology Development Organization (NEDO).

ORCID

Yuichi Oshima http://orcid.org/0000-0001-8293-4891
Takayoshi Oshima http://orcid.org/0000-0001-8550-9735

References

[1] Orita M, Ohta H, Hirano M, et al. H. Deep-ultraviolet transparent conductive β-Ga_2O_3 thin films. Appl Phys Lett. 2000;77(25):4166. doi: 10.1063/1.1330559
[2] Onuma T, Saito S, Sasaki K, et al. Valence band ordering in β-Ga_2O_3 studied by polarized transmittance and reflectance spectroscopy. Jpn J Appl Phys. 2015;54(11):112601. doi: 10.7567/JJAP.54.112601
[3] Higashiwaki M, Sasaki K, Kuramata A, et al. Gallium oxide (Ga_2O_3) metal-semiconductor field-effect transistors on single-crystal β-Ga_2O_3 (010) substrates. Appl Phys Lett. 2012;100(1):013504. doi: 10.1063/1.3674287
[4] Aida H, Nishiguchi K, Takeda H, et al. Growth of β-Ga_2O_3 single crystals by the edge-defined, film fed growth method. Jpn J Appl Phys. 2008;47(11):8506. doi: 10.1143/JJAP.47.8506
[5] Kuramata A, Koshi K, Watanabe S, et al. High-quality β-Ga_2O_3 single crystals grown by edge-defined film-fed growth. Jpn J Appl Phys. 2016;55(12):1202A2. doi: 10.7567/JJAP.55.1202A2
[6] Blevins JD, Stevens K, Lindsey A, et al. Development of large diameter semi-insulating gallium oxide (Ga_2O_3) substrates. IEEE Trans Semicond Manuf. 2019;32(4):466. doi: 10.1109/TSM.2019.2944526
[7] Galazka Z. Growth of bulk β-Ga_2O_3 single crystals by the Czochralski method. J Appl Phys. 2022;131(3):031103. doi: 10.1063/5.0076962
[8] Hoshikawa K, Kobayashi T, Matsuki Y, et al. 2-inch diameter (100) β-Ga_2O_3 crystal growth by the vertical Bridgman technique in a resistance heating furnace in ambient air. J Cryst Growth. 2020;545(May):125724. doi: 10.1016/j.jcrysgro.2020.125724
[9] Hoshikawa K, Kobayashi T, Ohba E, et al. 50 mm diameter Sn-doped (001) β-Ga_2O_3 crystal growth using the vertical bridgeman technique in ambient air. J Cryst Growth. 2020;546(June):125778. doi: 10.1016/j.jcrysgro.2020.125778
[10] Ueda Y, Igarashi T, Koshi K, et al. Two-inch Fe-doped β-Ga_2O_3 (010) substrates prepared using vertical Bridgman method. Jpn J Appl Phys. 2023;62(SF):SF1006. doi: 10.35848/1347-4065/acb55a
[11] Higashiwaki M, Konishi K, Sasaki K, et al. Temperature-dependent capacitance–voltage and current–voltage characteristics of Pt/Ga_2O_3 (001) schottky barrier diodes fabricated on n^-–Ga_2O_3 drift layers grown by halide vapor phase epitaxy. Appl Phys Lett. 2016;108(13):133503. doi: 10.1063/1.4945267
[12] Sasaki K, Wakimoto D, Thieu QT, et al. First demonstration of Ga_2O_3 trench MOS-Type schottky barrier diodes. IEEE Electron Device Lett. 2017;38(6):783. doi: 10.1109/LED.2017.2696986
[13] Dong P, Zhang J, Yan Q, et al. 6 kV/3.4 mΩ·cm^2 vertical β-Ga_2O_3 schottky barrier diode with $BV^2/R_{on,sp}$ performance exceeding 1-D unipolar limit of GaN and SiC. IEEE Electron Device Lett. 2022;43(5):765. doi: 10.1109/LED.2022.3160366
[14] Lin C-H, Ema K, Masuya S, et al. Uniformity improvement of thickness and net donor concentration in halide vapor phase epitaxial β-Ga_2O_3 wafers prepared on miscut angle substrates. Jpn J Appl Phys. 2023;62(SF):SF1005. doi: 10.35848/1347-4065/acb4fb
[15] Higashiwaki M, Sasaki K, Kamimura T, et al. Depletion-mode Ga_2O_3 metal-oxide-semiconductor field-effect transistors on β-Ga_2O_3 (010) substrates and temperature dependence of their device characteristics. Appl Phys Lett. 2013;103(12):123511. doi: 10.1063/1.4821858
[16] Li W, Nomoto K, Hu Z, et al. Single and multi-fin normally-off Ga_2O_3 vertical transistors with a breakdown voltage over 2.6 kV. In: 2019 IEEE International Electron Devices Meeting (IEDM) vol 2019-Decem IEEE. p.12.4.1–.12.4.4. doi: 10.1109/IEDM19573.2019.8993526
[17] Wong MH, Goto K, Murakami H, et al. Current aperture vertical β-Ga2O_3 MOSFETs fabricated by N- and Si-ion implantation doping. IEEE Electron Device Lett. 2019;40(3):431. doi: 10.1109/LED.2018.2884542
[18] Peterson C, Alema F, Bhattacharyya A, et al. Kilovolt-class β-Ga_2O_3 MOSFETs on 1-in. bulk substrates. Appl Phys Lett. 2024;124(8):082104. doi: 10.1063/5.0187989
[19] Wakimoto D, Lin C-H, Ema K, et al. A multi-fin normally-off β -Ga_2O_3 vertical transistor with a breakdown voltage exceeding 10 kV. Appl Phys Express. 2025;18(10):106502. doi: 10.35848/1882-0786/ae0d2a
[20] Sasaki K. Prospects for β-Ga_2O_3: now and into the future. Appl Phys Express. 2024;17(9):090101. doi: 10.35848/1882-0786/ad6b73
[21] Goto K, Konishi K, Murakami H, et al. Halide vapor phase epitaxy of Si doped β-Ga_2O_3 and its electrical properties. Thin Solid Films. 2018;666(September):182. doi: 10.1016/j.tsf.2018.09.006
[22] Ema K, Sasaki K, Kuramata A, et al. Homo- and hetero-epitaxial growth of β-gallium oxide via $GaCl_3$-O_2-N_2 system. J Cryst Growth. 2021;564(March):126129. doi: 10.1016/j.jcrysgro.2021.126129
[23] Fujikura H, Konno T, Yoshida T, et al. Hydride-vapor-phase epitaxial growth of highly pure GaN layers with smooth as-grown surfaces on freestanding GaN substrates. Jpn J Appl Phys. 2017;56(8):085503. doi: 10.7567/JJAP.56.085503

[24] Ahmadi E, Oshima Y. Materials issues and devices of α- and β-Ga_2O_3. J Appl Phys. 2019;126(16):160901. doi: 10.1063/1.5123213
[25] Oshima Y, Víllora EG, Shimamura K. Quasi-heteroepitaxial growth of β-Ga_2O_3 on off-angled sapphire (0001) substrates by halide vapor phase epitaxy. J Cryst Growth. 2015;410:53–58. doi: 10.1016/j.jcrysgro.2014.10.038
[26] Oshima Y, Oshima T. Rapid homoepitaxial growth of (011) β-Ga_2O_3 by HCl-based halide vapor phase epitaxy. Sci Technol Adv Mater. 2025;26(1):2585551. doi: 10.1080/14686996.2025.2585551
[27] Pechnikov AI, Stepanov SI, Chikiryaka AV, et al. Thick α-Ga_2O_3 layers on sapphire substrates grown by halide epitaxy. Semiconductors. 2019;53(6):780. doi: 10.1134/S1063782619060150
[28] Oshima Y, Oshima T. Homoepitaxial growth of (-102) β-Ga_2O_3 by halide vapor phase epitaxy. Semicond Sci Technol. 2023;38(10):105003. doi: 10.1088/1361-6641/acf241
[29] Oshima Y, Kawara K, Oshima T, et al. Rapid growth of α-Ga_2O_3 by HCl-boosted halide vapor phase epitaxy and effect of precursor supply conditions on crystal properties. Semicond Sci Technol. 2020;35(5):55022. doi: 10.1088/1361-6641/ab7843
[30] Goto K, Murakami H, Kuramata A, et al. Effect of substrate orientation on homoepitaxial growth of β-Ga_2O_3 by halide vapor phase epitaxy. Appl Phys Lett. 2022;120(10):102102. doi: 10.1063/5.0087609
[31] Murakami H, Nomura K, Goto K, et al. Homoepitaxial growth of β-Ga_2O_3 layers by halide vapor phase epitaxy. Appl Phys Express. 2015;8(1):015503. doi: 10.7567/APEX.8.015503
[32] Ema K, Lin C-H, Ueda Y, et al. Homo-epitaxial growth on the β-Ga_2O_3 (011) substrate by HVPE. In: Prenented in the 85th JSAP Autumn meeting 2024, presentation number 20p-A22-4 (abstract page 16–085);
[33] Hollar EJ, Farzana E. Over 3 kV and ultra-low leakage vertical (011) β -Ga_2O_3 power diodes with engineered schottky contact and high-permittivity dielectric field plate. Appl Phys Lett. 2026;128(5):053503. doi: 10.1063/5.0309746
[34] Wen J, Liu J, Li Q, et al. Over 3.5 kV (011) β-Ga_2O_3 schottky barrier diode and first demonstration of 4.7 kV nio-based (011) β-Ga_2O_3 heterojunction diode. In: 2026 IEEE 38th International Symposium on Power Semiconductor Devices and ICs (ISPSD). IEEE. p. 317–320. doi: 10.1109/ISPSD64561.2026.11553728
[35] Varley JB, Weber JR, Janotti A, et al. Oxygen vacancies and donor impurities in β-Ga_2O_3. Appl Phys Lett. 2010;97(14):142106. doi: 10.1063/1.3499306
[36] Shobu K. CaTCalc: new thermodynamic equilibrium calculation software. Calphad Comput Coupling Phase Diag Thermochem. 2009;33(2):279. doi: 10.1016/j.calphad.2008.09.015
[37] Yamaguchi H, Akito Kuramata TM. Slip system analysis and X-ray topographic study on β-Ga_2O_3. Superlattices Microstruct. 2016;99:99. doi: 10.1016/j.spmi.2016.04.030
[38] Oshima T, Oshima Y. Anisotropic non-plasma HCl gas etching of a (010) β-Ga_2O_3substrate. Appl Phys Express. 2023;16(6):66501. doi: 10.35848/1882-0786/acdbb7
[39] Oshima T, Oshima Y. Plasma-free dry etching of (001) β-Ga_2O_3 substrates by HCl gas. Appl Phys Lett. 2023;122(16):162102. doi: 10.1063/5.0138736